Supplementary Information

The formation and shape transformation mechanism of triangular Au nanoplate revealed by liquid-cell TEM

Biao Jin, [*a, b] Haifeng Wang, [c, d] Maria L. Sushko, [a] Chuanhong Jin [d] and Ruikang Tang [*b]

[a] Physical and Computational Sciences Directorate, Pacific Northwest National Laboratory, Richland, Washington 99354, United States

[b] Department of Chemistry, Zhejiang University, Hangzhou, Zhejiang 310027, China

[c] Institute of New Energy for Vehicles, School of Materials Science and Engineering, Tongji University, Shanghai 201804, China

[d] State Key Laboratory of Silicon Materials, School of Materials Science and Engineering, Zhejiang University, Hangzhou, Zhejiang 310027, China

*Correspondence to: biao.jin@pnnl.gov

rtang@zju.edu.cn

The PDF file includes:

Materials and Methods
Supplementary text
Supplementary Figures: Figures S1 to S4
Captions for Movie S1 to S3

Other supplementary materials for this manuscript includes the following:

Movie S1 to S3

Materials and Methods

Materials: $HAuCl_4 \cdot 3H_2O$ (Sigma-Aldrich) was used as received without further purification. $HAuCl_4$ was dissolved in ultrapure water (18.2 MΩ·cm) to prepare 100 mM stock solution and then diluted to 1.0 mM precursor solution prior to liquid cell transmission electron microscopy (LC-TEM) experiments.

Methods:

LC-TEM experiments.

(1) **In situ observations of Au NPLs formation process**: Investigating the early formation stage of nanoplate requires high spatial resolution , which means that thin liquid thickness and high electron dose rates were used. Here, we used K-kit liquid cell (BioMa-TEK) with 50 nm Si_3N_4 membranes and 200 nm gap distance to seal 1.0 mM $HAuCl_4$ precursor solution where only thin liquid film exists on the membrane to capture the early formation process of NPL with high resolution. The TEM-image time series were acquired with a software named Bandicam (Bandisoft) in a field emission FEI Tecnai G^2 F20 microscope (FEI) at 200 kV.

(2) **In situ observations of Au NPLs shape transition process:** All the chips were treated with oxygen plasma (20% vol. O_2 and 80% vol. N_2) in a Plasma Cleaner (Chendu Mingheng Science & Technology Co., Ltd, China) for 5 min to make the Si_3N_4 membranes surfaces hydrophilic prior to

use. For LC-TEM experiments, 400 nL 1.0 mM precursor solution was loaded into a liquid cell, which is consisted of spacer chip (100 nm gap) and blank chip with 50 μm × 200 μm and 50 nm thick Si_3N_4 membrane. It was assembled inside the liquid-cell holder (Hummingbird Inc. USA) so that an integrated liquid cell with electron-transparent window was completed. The leak checking of liquid cell was performed prior to TEM. After that, the liquid cell holder was put into TEM for observation. A field emission FEI Tecnai G^2 F20 microscope (FEI, USA) operated at 200 kV for in situ TEM imaging with low electron dose rate with 4.8 e/$Å^2$s. The TEM-image time series were acquired with an OneView camera (Gatan, Inc., Pleasanton, CA, USA).

Simulations

(1) Density Functional Theory (DFT) simulations. Plane wave DFT simulations were used to determine the energetics of Au adatom deposition onto a concave and convex edges of Au nanoparticle. Simulations were performed using DFT with PBE exchange-correlation functional[1] and projector augmented wave potentials, as implemented in the VASP code.[2, 3] The plane-wave basis with a 500 eV cutoff and a Gamma-centered 3 × 3 × 3 Monkhorst–Pack grid were used. Au nanoparticle with concave and convex edge and (111) top and bottom surfaces was modelled as a 106- and 184-atom slabs, respectively, and a 15 Å vacuum gap was used to avoid interactions between the slabs. Two bottom Au layers were fixed at their bulk positions to emulate the atomic positions in the middle of the nanoparticle. All other atoms were fully relaxed. Previous studies demonstrated a fast convergence of the surface energies with slab thickness with fully converged values obtained for a 5-layer slab.[4] In this work the slab thickness varies between 7 and 13 layers depending on the position across the edge. Fermi method with a width of 0.2 eV was used for electronic smearing.

(2) **Modified kinetic Wulff model.** Simulations of thermodynamic and kinetic particle shape were performed using the modified kinetic Wulff model and kineticGUI software.[5] The following scaled surface energies or growth velocities for the {100}, {110}, and {111} surfaces were used for thermodynamic and kinetic modeling of monotwinned Au crystals, respectively: $\gamma_{100} = 9.61$, $\gamma_{110} = 14.42$, $\gamma_{111} = 0.961$. The enhancement factors of $\varphi_{twin}(\vec{n}) = 2.16$, determined using DFT simulations, and $\varphi_{re-entrant}(\vec{n}) = 2.0$ were used.

Supplementary text

Determination of side faces structures of NPL

As described in previous works, the side faces structures of NPL are elusive, despite a speculation of a mixture of {100} and {111} facets. In order to understand the mechanism of shape transition, we disassembled the liquid cell and then check these NPLs structure by TEM. Figure 4a shows the TEM image and corresponding SAED pattern of a triangular NPL along the [111] zone axis, which indicates that NPL contains single {111} facets on their two planar surfaces. Besides the six bright diffraction spots in a 6-fold symmetry corresponding to {220} facets, theoretically forbidden 1/3{422} reflections match with the characteristics of {111} twin facets oriented parallel to the NPL surface. To obtain the information on side-faces structure, tilting experiments were conducted on individual NPL. When the triangular NPL was titled by ~35°, the SAED pattern was observed along the [011] zone axis (Figure 4b). Since {100} diffraction spots which correspond to the side-edge used as the titling axis appear in

the SAED pattern and the angle between the {011} and {111} facets is 90°, the corresponding side facets of triangular NPL should include {100} and {111} facets. Overall, these results enable us to ascertain a geometrical model of NPLs, in which each NPL was enclosed by two {111} facets as the top and bottom faces, and by a mix of {100} and {111} facets as the side faces, as schematically illustrated in Figure 4c.

Supplementary Figures: Figures S1 to S4

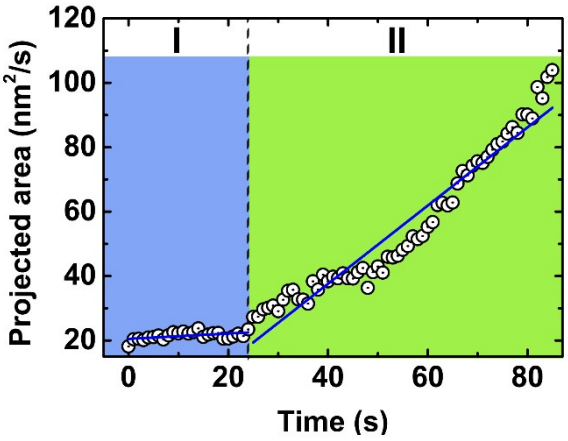

Figure S1. Projected area of nanocrystal versus growth time, as the case shown in movie S1.

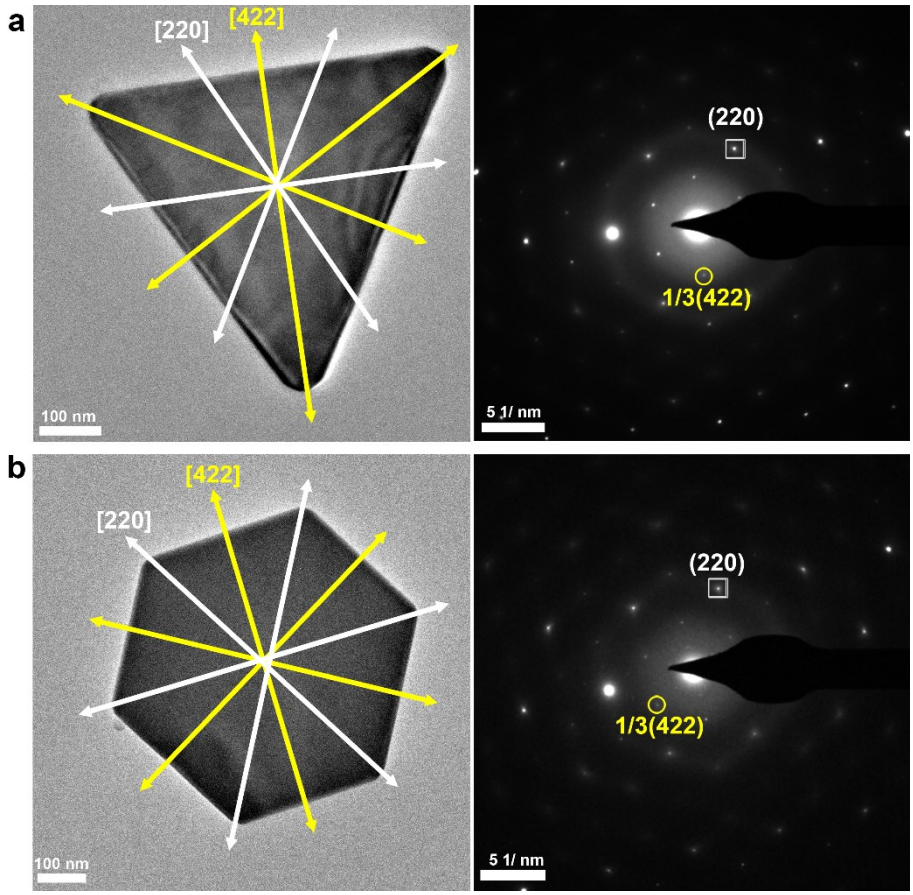

Figure S2. Ex situ HRTEM and SAED analyses of the gold NPL synthesized on the Si_3N_4 membrane in the liquid-cell TEM experiments. (a) gold triangular NPL, (b) hexagonal NPL. The [220] and [422] crystallographic directions are indicated by white and yellow lines, respectively.

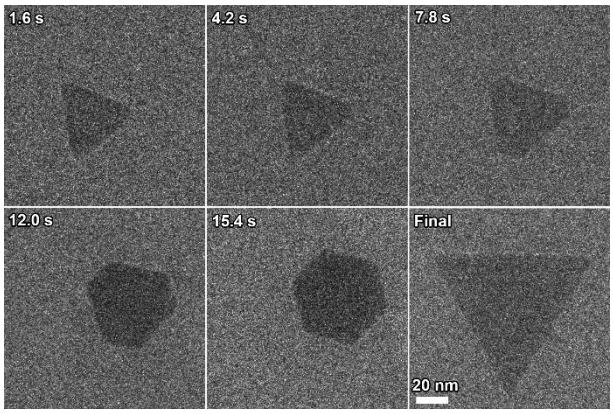

Figure S3. Time-lapse sequence of in situ TEM images shows the transformation of triangular to hexagonal to final reversed triangular nanoplate.

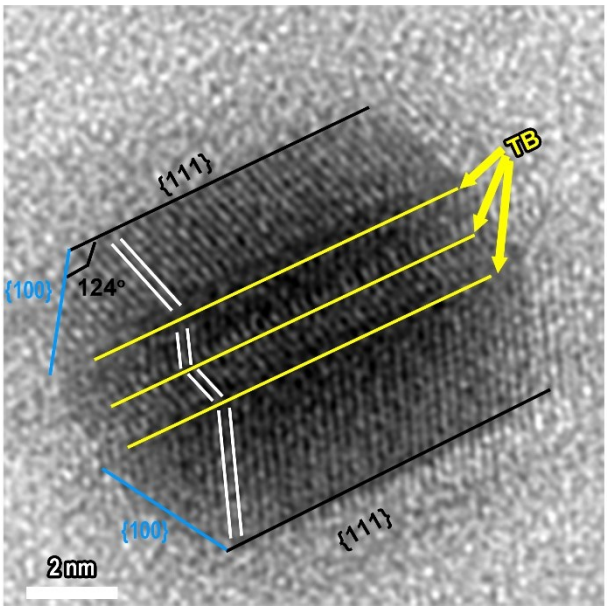

sFigure S4. The side structure of triangular Au NPL, showing the existence of both {100} and {111} faces.

Captions for Movie S1 to S3

Movie S1

Representative bright field TEM movie showing the formation of Au triangle NPL in 1.0 mM $HAuCl_4$ in the liquid cell. The electron dose rate is 15900 $e^-/Å^2 \cdot s$. Graphical data shown in Figure 1a, main text. The video plays at 5X normal speed.

Movie S2

Representative bright field TEM movie showing the formation of Au triangle NPL in 1.0 mM $HAuCl_4$ in the liquid cell. The electron dose rate is 4190 $e^-/Å^2 \cdot s$. Graphical data shown in Figure 1b, main text. The video plays at 5X normal speed.

Movie S3

Typical bright field TEM movie showing the shape evolution of Au NPL in 1.0 mM $HAuCl_4$ in the liquid cell. The electron dose rate is 4.8 $e^-/Å^2 \cdot s$. Graphical data shown in Figure 3, main text. The video plays at 4X normal speed.

References

1. Perdew, J. P.; Burke, K.; Ernzerhof, M. *Phys. Rev. Lett.* **1997,** 78, (7), 1396-1396.
2. Kresse, G.; Hafner, *Phys. Rev. B* **1993,** 48, (17), 13115-13118.
3. Kresse, G.; Furthmuller, *Phys. Rev. B* **1996,** 54, (16), 11169-11186.
4. Almora-Barrios, N.; Novell-Leruth, G.; Whiting, P.; Liz-Marzan, L. M.; Lopez, N. *Nano Lett.* **2014,** 14, (2), 871-875.
5. Ringe, E.; Van Duyne, R. P.; Marks, L. D. *J. Phys. Chem. C* **2013,** 117, (31), 15859-15870.